

Bringing IoT to Sports Analytics

Mahanth Gowda¹, Ashutosh Dhekne^{1,†}, Sheng Shen^{1,†}, Romit Roy Choudhury¹, Xue Yang², Lei Yang², Suresh Golwalkar², and Alexander Essanian²

¹University of Illinois at Urbana-Champaign

²Intel

[†]*Co-secondary authors*

Abstract

This paper explores the possibility of bringing IoT to sports analytics, particularly to the game of Cricket. We develop solutions to track a ball’s 3D trajectory and spin with inexpensive sensors and radios embedded in the ball. Unique challenges arise rendering existing localization and motion tracking solutions inadequate. Our system, *iBall*, mitigates these problems by fusing disparate sources of partial information – wireless, inertial sensing, and motion models – into a non-linear error minimization framework. Measured against a *mm*-level ground truth, the median ball location error is at 8cm while rotational error remains below 12° even at the end of the flight. The results do not rely on any calibration or training, hence we expect the core techniques to extend to other sports like baseball, with some domain-specific modifications.

1 Introduction

Sports analytics is a thriving industry in which motion patterns of balls, racquets, and players are being analyzed for coaching, strategic insights, and predictions. The data for such analytics are sourced from expensive high-quality cameras installed in stadiums, processed at powerful backend servers and clouds. We explore the possibility of significantly lowering this cost barrier by embedding cheap Inertial Measurement Unit (IMU) sensors and ultrawide band (UWB) radios inside balls and players’ shoes. If successful, real-time analytics should be possible anytime, anywhere. Aspiring players in local clubs could read out their own performance from their smartphone screens; school coaches could offer quantifiable feedback to their students.

Our work follows a growing excitement in IoT based sports analytics. Sensor-enabled football helmets, aimed at detecting concussions and head injuries, are already in the market. Nike is prototyping IMU-embedded shoes [34, 47], while multiple startups are pursuing ideas around camera-embedded jerseys [5], GPS-enabled soccer balls [6], and bluetooth frisbees [1]. However, we have not found a serious effort to accurately characterize 3D ball motion, such as trajectory, orientation, revolutions per second, etc.

The rich literature in wireless localization and inertial

gesture recognition does not apply directly. WiFi-like localization infrastructure is mostly missing in the playground, and even if deployed, is not designed to support *cm-scale* 3D location at ball speeds. Inertial sensors such as accelerometers do not measure gravity when the ball is in free fall, since these sensors detect only reactive forces. Worse, gyroscopes saturate at around 6 revolutions per second (rps) [8], while even an amateur player can spin the ball at 12rps. In general, tracking a fast moving/spinning object in an open playground presents a relatively unexplored context, distinct from human-centric localization and gesture tracking applications.

In approaching this problem top-down, we develop multiple wireless and sensing modules, and engineer them into a unified solution. The technical core of our system relies on using ultrawide band (UWB) radios to compute the time of flight (ToF) and angle of arrival (AoA) of the signals from the ball. When this proves inadequate, we model the ball’s physical motion as additional constraints to the underdetermined system of equations. Finally, we fuse all these sources of information into a non-linear error minimization framework and extract out the parameters of ball trajectory.

Spin estimation poses a different set of challenges. We need to determine the initial orientation of the ball at its release position and then track the 3D rotation through the rest of the flight. With unhelpful accelerometers and gyroscopes, we are left with magnetometers. While magnetometers do not capture all the dimensions of rotation, we recognize that the uncertainty in the ball’s spin is somewhat limited since air-drag is the only source of torque. This manifests on the magnetometer as a sinusoidal signal, with a time varying bias (called “wobble”). We formulate this as a curve-fitting problem, and jointly resolve the ball’s angular velocity as well as “wobble”. In general, we learn that magnetometers can serve as gyroscopes in free-spinning objects.

Our experiment platform is composed of an Intel Curie board (IMU + UWB) embedded in the ball by a professional design company [3]. Two small UWB receiver boxes, called *anchors*, are also placed on the ground – additional anchors are infeasible due to the field layout

in the Cricket game, discussed shortly. For ground truth, we use 8 Vicon based IR cameras positioned at 4 corners of the ceiling. IR markers are pasted on the ball to enable precise tracking (0.1mm and 0.2° for location and orientation). Since the ViCon coverage area is $10 \times 10 \times 4\text{m}^3$ – around half of the actual Cricket trajectories – we scale-down the length of the throws while maintaining realistic speed and spin.

Reported results from 100 different throws achieve median location accuracy of 8cm and orientation errors of 11.2° , respectively. A player (wearing a clip-on UWB board) is also tracked with a median error of 1.2m even when he is at the periphery of the field (80m away from the anchor). All results are produced at sub-second latency, adequate for real time feedback to human players.

There is obviously room for continued research and improvement. First, we have sidestepped the energy question. In future, perhaps wireless charging will mitigate this problem; perhaps fast rotation will automatically scavenge energy. For now, our solution allows a battery life of ≈ 75 minutes between re-charges, permitting short training sessions. Second, our aerodynamic motion models are simplistic and did not get stress-tested in indoor settings– this may have yielded favorable results. Moreover, we could not exceed throw speeds beyond 45 miles/hour and 12 revolutions/s, both of which are around half of the professionals. Finally, this paper focuses on Cricket, and although we believe our techniques are generalizable with modest modifications, we have not verified these claims. Our ongoing work is focussed on adapting *iBall* to baseball and frisbee.

To summarize, the contributions of this paper are:

- *Formulating object tracking as an information fusion problem under the practical constraints of Cricket.* Designing an optimization framework for fusing time of flight (ToF) measurements, air-drag motion models, and noisy angle of arrival (AoA) estimates, to ultimately achieve desired accuracy.
- *Identifying various opportunities arising from free-fall motion.* Harnessing the magnetometer to jointly estimate rotation and rotation axis, thereby emulating an inertial gyroscope in free-fall scenarios.

The rest of the paper expands on these technical components woven together by significant engineering effort. We begin with some background on Cricket, followed by challenges, opportunities, design, and implementation.

2 Background and Platform

2.1 Quick Primer on Cricket

We summarize the basic rules of cricket for those unfamiliar with the game. A Cricket match is divided into

two sessions – in any session, one team is called the *batting side* and the other is called the *bowling or fielding side*. The teams switch roles in the second session. A playing *pitch* is located at the center of the field, with two *wickets* on each side of the pitch. A wicket is a set of 3 wooden sticks placed vertically one beside the other (see Fig.1). A player from the batting side stands in front of a *wicket* while a player from the bowling side runs up to the other wicket and throws the ball towards the batsman. All other players of the bowling side are called *fielders* and stand scattered around the park.

The bowler's objective is to hit the wicket with the ball, or to force the batsman to hit the ball in a way that a fielder can *catch* the ball before it drops to the ground. If the bowler is successful, the batsman is *out*, i.e., he goes off the field and the next batsman of the batting team comes to face the bowler. The batsman's goal, on the other hand, is to not get out, and to also hit the ball so that it goes past the fielders and reaches the periphery of the park, called a *boundary*. If the ball bounces on the ground at least once before it crosses the boundary, then the batting side scores 4 more points (called *runs*); if the ball goes over the boundary without any bounce, 6 runs are added to the team's score. A session ends when either N deliveries have been bowled or all the 11 batsmen are out, whichever occurs earlier. At the end, the team with a higher total score wins.

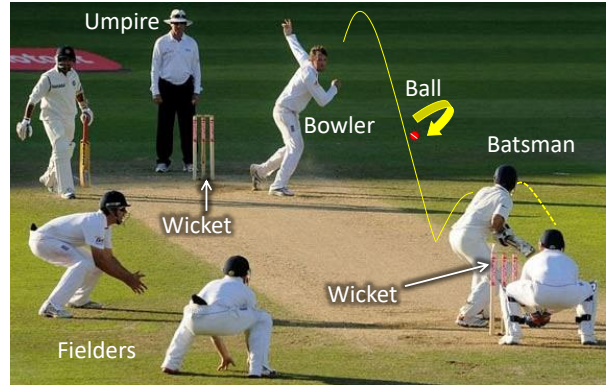


Figure 1: Cricket in action. Two sets of wickets placed at the bowler's and batsman's end.

Analogy to Baseball: The similarity between Cricket and Baseball, from the perspective of ball and player tracking, is noteworthy. The baseball travels and spins at comparable speeds and rates, while the length of the “pitch” is also similar. Differences might arise from the stitching patterns on the ball, and the viability of placing multiple anchors in baseball (in contrast to 2 in Cricket). In this sense, perhaps the ball's trajectory tracking problem becomes simpler in the case of baseball, but the spinning question still remains relevant.



Figure 2: Ball instrumentation: (a) Intel Curie board with IMU sensors and UWB radio. (b) Scooped out cricket ball for snug fit of the sensor box. (c) Closed ball with sensor box. (d) UWB 4-antenna MIMO radio serving as an anchor.

2.2 The Solution Space

There are obviously many approaches to ball and player tracking – we briefly discuss our deliberations for selecting the IMU/UWB platform.

- High end camera networks used today are expensive (\$100,000+) because they need to be far away [9], hence, we considered placing cheaper cameras at the wickets. The benefit is that the ball need not be instrumented. However, with no markers on the ball, spin tracking and de-blurring is challenging even with the best cameras. Cheap cameras at the wickets experience similar problems, get occasionally occluded by players, suffer in low light, and cannot track fielders scattered in the field. Experiments with iPhone cameras yielded poor results even with colored tapes on the ball.
- RFIDs on the ball (and readers placed at wickets) pose a far less price point (\$2000). However, the rapidly spinning RFIDs exhibit continuous disconnections [44]. Further, cricket balls are continuously rubbed to maintain shine, crucial to the ball’s swing and spin – pasting antennas on the surface is impractical.
- WiFi based tracking solutions are also impractical under the constraints of high speed and spin, cm-scale accuracy, and availability of a very few base stations on the 2D ground (which makes 3D tracking difficult due to *dilution of precision* (DoP) [26, 39]). Trials with laser rangers [22] and acoustic reflection techniques [20] also proved pointless. Given the small cross-sectional area of the ball, the reflections from them yielded high false positives.
- Our choice to embed electronics in the ball, although cumbersome, proved practical for accuracy and coverage in the field. In discussion with 3D printing and design companies, we gained confidence that embedding should be feasible even under impact. Finally, UWB radios offer time of flight capabilities, a pre-requisite for extremely fast moving balls ($> 80+$ miles/hour). Our overall cost is estimated at \$250.

2.3 Instrumenting Balls and Anchors

Fig.2 illustrates the steps in ball instrumentation. A Quark CPU, IMU BMM150 sensors, and a Decawave UWB radio are cased in a plastic polymer box and snug-fitted into a hole (to avoid rattling). The two halves of the ball are closed shut and a hole drilled to bring out a USB port to the surface for recharging. The sensor data is stored on a local flash or can be streamed through the UWB radio to the nearby “anchor”.

The anchor is a UWB receiver box placed at each wicket. The UWB radio from Decawave [4] is 802.15.4 compliant with support for 3.5 to 6.5 GHz bands (12 channels) and a bandwidth of 500 MHz (data rates of up to 6.8 Mbps). The radio operates under low power, with sleep current at 100 nanoAmp. While the ball contains a single antenna (due to space restrictions), a 4 antenna MIMO radio is fitted in the anchor (Fig.2(c)).

Fig.3 illustrates the overall deployment in real settings. UWB signals are exchanged between the ball and anchors to compute the ball’s range as well as the angle of arrival (AoA) from the phase differences at different antennas. The range and AoA information are combined for trajectory estimation. For spin analytics, the sensors inside the ball send out the data for off-ball processing. Players in the field can optionally wear the same IMU/UWB device (as in the ball) for 2D localization and tracking.

3 System Design: 3D Spin Tracking

Three main spin-related metrics are of interest to Cricketers: (1) revolutions per second, (2) rotation axis, and (3) seam plane¹. From a sensing perspective, all these 3 metrics can be derived if the ball’s 3D orientation can be tracked over time. This motivates a discussion on orientation, rotation, and coordinate frameworks.

¹The seam is a stitch along the equator of the Cricket ball.

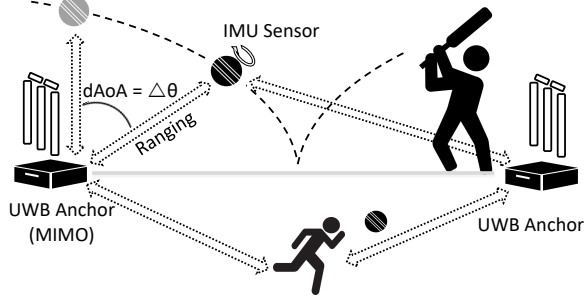


Figure 3: Two anchors and a ball deployed on the ground, while players optionally have the device in their shoes.

3.1 Foundations of Orientation

The *orientation* of an object is the representation of the object’s local X, Y, Z axes as vectors in the global coordinate frame. A *rotation* of an object is a change of orientation, and can be decomposed into sequence of rotations around its (local) X, Y, and Z axes. Put differently, any new orientation can be achieved by rotating the object (by appropriate amounts) on each of the 3 axes, one after the other. The gyroscope measures each of these rotations per unit time, called *angular velocity*. Thus, theoretically, if one knows the *initial orientation* of an object in the global coordinate frame, then subsequent orientations can be tracked by integrating the gyroscope-measured angular velocity across time.

Expressing the object’s initial orientation in the global framework should be possible since gravity and magnetic North are both along globally known directions. Thus, the object’s local axes can be rotated until the local representation of gravity and North align with the known global directions. We consider an example below.

Fig.4(a) shows a global frame $\{X_g, Y_g, Z_g\}$ with its X_g pointing East, Y_g pointing North, and Z_g pointing up against gravity. Fig.4(b) shows an object in an unknown orientation. Now, the object can be rotated around X axis until the measured gravity is along its own $-Z$ direction; it can be rotated again around this $-Z$ axis until the measured magnetic field (compass) is along its own Y . Now the local and global frameworks have fully aligned, and we denote the total rotation as a single matrix R :

$$[X \ Y \ Z] R = [X_g \ Y_g \ Z_g]$$

We define an object’s orientation, R_O , as the inverse of this rotation matrix, R^{-1} . Intuitively, if an object needs a clockwise rotation of 30° to align with the global framework, then its orientation must be 30° counter-clockwise. Thus, we have the capability to compute both initial orientation and angular velocity; from these, any spin-related analytics should ideally be trackable.

■ Challenges with In-Flight Balls: Challenges emerge in the real world and particularly in this cricket setting:

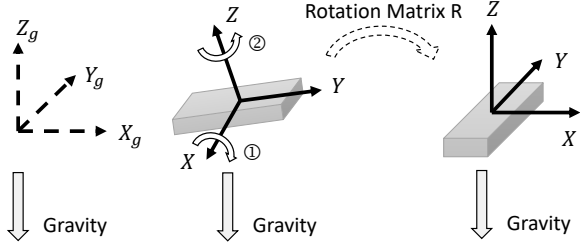


Figure 4: Rotating local axes to align local directions of gravity and magnetic North with the global directions.

(1) The gyroscope is noisy and this error accumulates since rotation is a time-integral of angular velocity (2) Worse, the gyroscope saturates beyond 5 revolutions/sec. (rps), while even amateurs can spin the ball at 12 rps (professionals attain > 30). (3) Finally, gravity is not measured in accelerometers during free-fall which precludes opportunities to rotate and align the local coordinate frame². In sum, known techniques cannot compute initial orientation or rotation when the ball is in flight.

3.2 The Core Opportunity

At a high level, 2 observations are central.

- In the absence of air-flow, there is no external torque on the ball, implying that the ball’s rotation is restricted to a single axis throughout the flight (i.e., the axis around which it was rotated by the bowler).
- From the ball’s local reference frame, the magnetic North vector spins around some axis. Given a single rotation axis, the magnetometer can indeed infer the axis and measure both magnitude and direction of rotation.

Of course, air-drag pollutes this opportunity since the ball begins to experience additional rotations. This poses the main challenge. An illustrative example follows.

3.3 An Illustrative Example

Let’s assume the ball’s mass is symmetrically distributed and its center of mass is precisely at the center. Let’s also consider gravity forces alone and no air drag. Now, due to conservation of angular momentum, the ball will not change its rotating state because no torque is generated from gravity. The dimension of this rotational motion is limited to 1 since the motion can be continuously expressed around a single axis, R^G . Fig.5 illustrates the situation – each local X, Y, Z axis rotates in different cones

²A full analysis of IMU deficiencies is outside the scope of this paper. Briefly, gyroscope saturation is rooted in imperfections accumulated during the manufacturing process of MEMS sensors. These imperfections make gyroscopes exhibit nonlinear responses to input vibrations [48, 40], and attempts to reduce imperfections increases cost or lowers yield rate. Accelerometers on the other hand are fundamentally designed to measure reactive forces, and hence, do not sense gravity during free fall.

around the same R^G . As an aside, the magnetic North is also a fixed vector N^G in the global framework (henceforth, we use superscript G/L to indicate that a vector is being observed in the global/local framework).

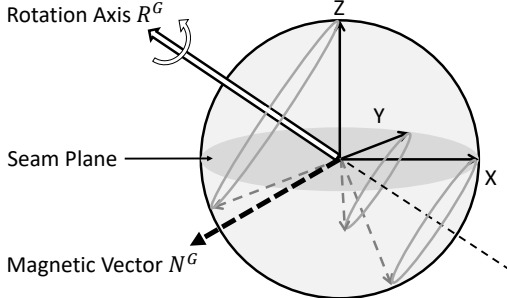


Figure 5: In the global framework, the ball is rotating around a constant rotation axis R^G .

Shifting our perspective from the global to local coordinate system, Fig.6(a) shows that the local X, Y, and Z axes are now fixed, but the magnetic vector N^L rotates in a cone around a fixed local vector R^L . Since magnetometers can reliably measure a single dimension of rotation, it should be possible to measure the parameters of this cone. This is the core opportunity – the low-dimensional mobility during free-fall empowers the magnetometer to serve as a gyroscope.

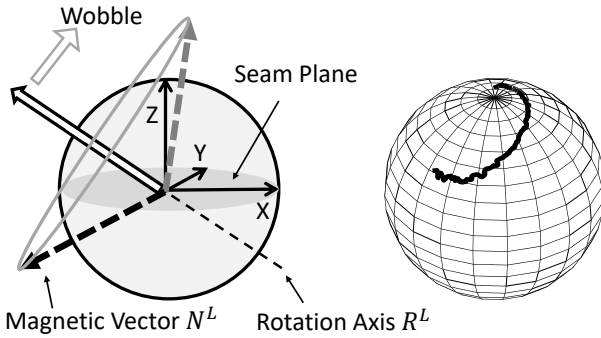


Figure 6: (a) In the local framework, the magnetic vector N^L is rotating around local rotation axis R^L . (b) In the local framework, local rotation axis R^L is slowly moving

Unfortunately, with air-drag, the ball still continues to rotate around the same global axis R^G , but experiences an additional rotation along a changing axis. To envision this, consider the ball spinning around the global vertical axis with the seam on the horizontal plane. With air-drag, the ball can continue to spin around the identical vertical axis, but the seam plane can gradually change to lie on the vertical plane. This is called “wobble” and can be modeled as a varying local rotation axis, R^L . Fig.6(b) shows the locus of R^L as it moves in the local framework

(this was derived from ViCon ground truth). Thus, the center of the N^L cone is moving on the sphere surface, even though the width of the cone remains unchanged. This derails the ability to compute rotations from magnetometers.

3.4 Problem Formulation

Based on the earlier discussion, we know that if two non-collinear vectors can be observed in the local framework, and their representations known in the global frame, then the orientation of the object can be resolved. We mathematically express the orientation of the ball at time t as a rotation matrix, $R_{O(t)}$. This matrix is a function of the globally fixed vectors (i.e., rotation axis and magnetic North) and their locally measured counterparts.

$$R_{O(t)} = [R^G \quad N^G \quad R^G \times N^G] [R_{(t)}^L \quad N_{(t)}^L \quad R_{(t)}^L \times N_{(t)}^L]^{-1} \quad (1)$$

Here R^G and N^G are the rotation axis and magnetic North vectors, respectively – both are in the global framework and are constant during flight. The third column vector, $(R^G \times N^G)$, is a cross product necessary to equalize the matrix dimensions on both sides. $N_{(t)}^L$ is the local magnetic vector measured by the magnetometer, $[m_x \ m_y \ m_z]^T$. $R_{(t)}^L$ is the local rotation axis which is slowly changing during the flight of the ball. From previous discussion we know that $R_{(t)}^L$ is always the centerline of the instantaneous $N_{(t)}^L$ cone.

Our goal now is to estimate two of the unknowns, namely R^G and time varying $R_{(t)}^L$. We know that R^G remains constant hence resolving it at the beginning of the flight will suffice – the same value can be used all the way till the end. For $R_{(t)}^L$, we know that it is moving on the sphere of the ball and the magnetic North is constantly rotating around it. We focus on tracking $R_{(t)}^L$ first and then address R^G .

3.5 Tracking Local Rotation Axis $R_{(t)}^L$

Since $N_{(t)}^L$ forms a cone around $R_{(t)}^L$, tracking $R_{(t)}^L$ is equivalent to tracking the centerline of the cone. Now, given that 3 non-coplanar unit vectors determine a cone, a straightforward idea is to fit a cone using 3 consecutive measurements: $N_{(t-1)}^L$, $N_{(t)}^L$ and $N_{(t+1)}^L$. Fig.7 shows the result: the estimation follows the true $R_{(t)}^L$ trend, but is considerably noisy.

These noise in $R_{(t)}^L$ estimation will translate to orientation error according to Equation 1. The noise cannot be reduced by fitting the cone over larger number of magnetometer measurements – this is because the cone would have moved considerably within a few sampling intervals. Our observation is that, because the ball’s flight

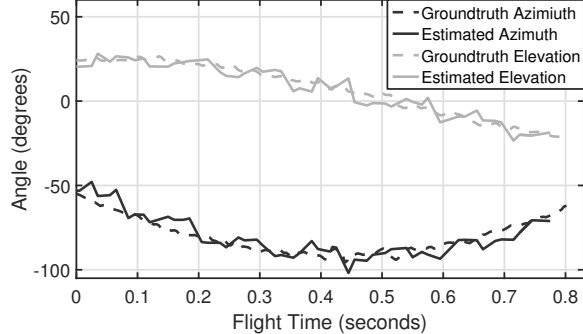


Figure 7: One example of $R_{(t)}^L$ estimation from cone fitting

time is short (less than a second), we can effectively describe the (azimuth and elevation³) changes in $R_{(t)}^L$ as a quadratic function of time t . Formally:

$$R_{(t)}^L = \begin{bmatrix} \cos(\theta_t) \cos(\varphi_t) \\ \cos(\theta_t) \sin(\varphi_t) \\ \sin(\theta_t) \end{bmatrix}$$

$$\text{Elevation } \theta_t = A_{el} t^2 + B_{el} t + C_{el}$$

$$\text{Azimuth } \varphi_t = A_{az} t^2 + B_{az} t + C_{az}$$

Put differently, we model the motion of a moving cone, under the constraints that the center of cone is moving on quadratic path (on the surface of the sphere) and that the cone angle $\theta_{NR} = \angle(N_{(t)}^L, R_{(t)}^L)$ is constant. We pick the best 6 parameters of this model that minimize the variance of the cone angles as measured over time. Our objective function is:

$$\underset{6 \text{paras}}{\operatorname{argmin}} \operatorname{Var} \left[\angle(R_{(T)}^L, N_{(T)}^L), \angle(R_{(T+1)}^L, N_{(T+1)}^L), \dots \right] \quad (2)$$

where T is the moment the ball is released. The initial condition to this optimization function is derived from a smoothed version of the basic cone fitting approach, described in Fig.7.

3.6 Track Global Rotation Axis R^G

Fig.8 shows 2 phases of ball tracking: *pre-flight* and *in-flight*. The above section described phase 2, the tracking of $R_{(t)}^L$ when the ball is spinning *in-flight*. However, recall that the global rotation axis, R^G , also needs to be estimated to solve for orientation $R_{O(t)}$ in Equation 1. Tracking R^G during the ball's flight is difficult. Sensor data during the flight only tells us where $R_{(t)}^L$ is pointing (center of the $N_{(t)}^L$ cone) but it does not reveal any information about R^G . Fortunately, the rotation axis R^G and

³Azimuth and elevation are latitudinal and longitudinal directions on a sphere's surface: a point on the sphere can be expressed as a tuple of these 2 angles.

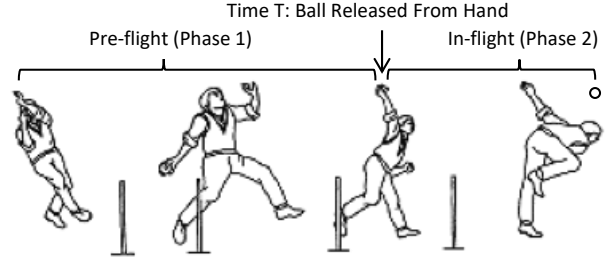


Figure 8: Two phases of ball motion.

magnetic vector N^G are two constant vectors. The angle between these two vectors, $\angle(N^G, R^G)$ is the same as the local $N_{(t)}^L$ cone angle θ_{NR} . Thus, R^G can only lie on a cone around N^G whose cone angle is θ_{NR} . Although useful, it's insufficient – we still do not know the point on the cone's circle corresponding to R^G .

To mitigate this problem, we focus on sensor measurements in phase 1 (pre-flight). Since this is not free-fall, and the ball is not spinning fast, the gyroscope and accelerometer are both useful. Our aim is to identify a stationary time point to compute the initial orientation of the ball, and use the gyroscope thereafter to integrate rotation until the point of release, T . Once we obtain orientation at T , denoted $R_{O(T)}$, we simply use the following equation to solve for the global rotation axis $R_{(T)}^G$

$$R_{(T)}^G = R_{O(T)} R_{(T)}^L \quad (3)$$

Then, we use $R_{(T)}^G$ as our estimation of R^G for the whole flight in Phase 2.

In general, gyroscope noise and saturation can render $R_{(T)}^G$ erroneous. However, since the ball does not spin while in the hand (in fact, it rotates less than 1 revolution), and the angular velocity saturates the gyroscope only at the last few moments before ball-release, we calibrate $R_{(T)}^G$ using the cone angle restriction mentioned above. Fig.9 reports consistently small $R_{(T)}^G$ error from 50 experiments.

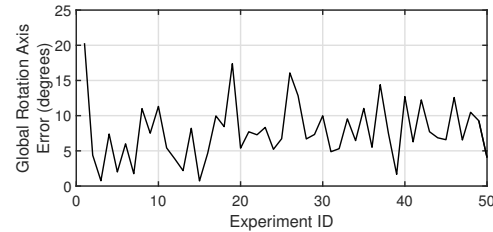


Figure 9: Error in estimating global rotation axis $R_{(T)}^G$ is reasonably small across 50 experiments.

In conclusion, gyroscope dead-reckoning right before ball release, combined with local rotation axis tracking

during flight, together yields the time-varying orientation of the ball. Algorithm 1 presents the pseudo code for final overall solution.

Algorithm 1 Ball Orientation Tracking During Flight

- 1: Get coarse $R_{(t)}^L$ by combining 3 consecutive magnetometer measurements
- 2: Use them as the initial starting point to search for parameters that minimize $\text{Var}[N_{(t)}^L \text{ cone angles}]$
- 3: Compute cone angle $\theta_{RN} = \text{Mean}[N_{(t)}^L \text{ cone angles}]$
- 4: Use gyroscope to tracking ball's orientation at the release time, $R_{O(T)}$
- 5: Get global rotation axis during flight:

$$R^G = R_{O(T)} R_{(T)}^L$$
- 6: Calibrate R^G using θ_{RN} .
- 7: Use Equation 1 to compute ball's orientation at any time t during flight

4 System Design: 3D Trajectory Tracking

Location related analytics are also of interest in Cricket. 3 main metrics are: (1) distance to first bounce, called *length*, (2) direction of ball motion, called *line*, and (3) *speed* of the ball at the end of the flight. These metrics are all derivatives of the ball's *3D trajectory*. Our approach to estimating 3D trajectory relies on formulating a parametric model of the trajectory, as a fusion of the *time of flight* (ToF) of UWB signals, *angle of arrival* (AoA), physics motion models, and DoP constraints (explained later). A gradient decent approach minimizes a non-linear error function, resulting in an estimate of the trajectory. We present technical details next.

4.1 Ranging with UWB

The Decawave UWB radios offer time resolution at 15.65ps . With modest engineering, we were able to compute the ToF and translate it to range measurements (with 15cm error). Briefly, the ball sends a POLL, the anchor sends back a RESPONSE, and the ball responds with a FINAL packet. Using the two round trip times, and the corresponding turn-around delays, the time of flight is computed without requiring time synchronization between the devices (algorithm details in [21, 4]). Multiplied by the speed of light, this yields the ball's range. This is not our contribution since the Decawave platform offers the foundational capabilities.

Observe that UWB ranging is available from only 2 anchors (placed at the two wickets) and therefore inadequate to resolve the 3D location of the ball. Additional anchors cannot be placed on the ground since it will interfere with the motion of the ball and fielders, while

placing anchors outside the field (90m away from the wickets) significantly degrades SNR and ranging accuracy. Fig.10 shows the intersections of the 2 anchor measurements, i.e., circles formed by the intersection of two spheres centered at the anchors. At a given time, the ball can lie on any point of a circle. Given that the initial position and velocity of the ball is unknown, many 3D trajectories can satisfy these constraints.

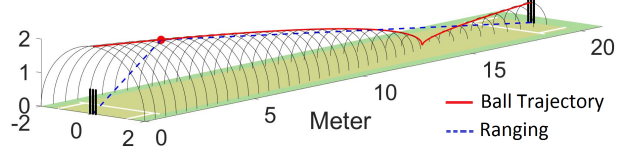


Figure 10: Intersections of ranging measurements leave one location dimension unresolved.

4.2 Mobility Constraints

We bring two mobility constraints to resolve the uncertainty: (1) physics of ball motion, and (2) opportunities from the ball's bouncing position.

(1) Physics of Ball Motion

Fig.11 shows a free-body diagram depicting the forces acting on the Cricket ball while in flight. Besides gravity, aerodynamic forces are acting on the ball. Briefly, the ball surface is smooth on one side of the seam and rough on the other (Cricket bowlers continue to polish the smooth side during the game). This disparity causes unbalanced air-flow, causing a side force. The speed of the ball can cause a slight air drag force. The magnitude and direction of the side forces depends on the seam orientation, surface roughness, and ball velocity. The drag and side force coefficients can be approximated as constants [14]. The side force can produce up to 1m of lateral deflection in trajectory.

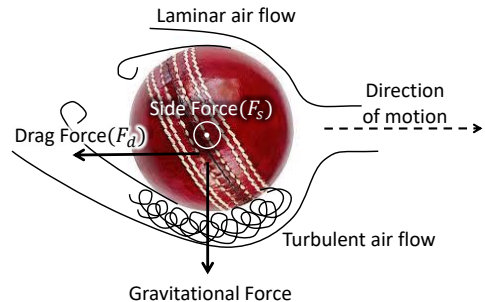


Figure 11: Unbalanced air-flow due to asymmetric smoothness on the ball's surface causes side force.

Under the above forces, ball motion follows a simple projectile path [14].

Fig.12(a) shows the extent to which the projectile model (without the aerodynamic forces) fits the ball's true tra-

jectory (derived from ViCon). The projectile was seeded by the ViCon-computed initial location and initial velocity. The median error is 1cm across 25 different throws of the ball, offering confidence on the usability of the model in indoor environments. The efficacy outdoors remains an open question.

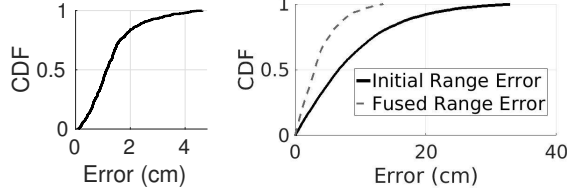


Figure 12: (a) Error between a parametric motion model and ground truth (derived from ViCon cameras). (b) Reduced ranging error after fusing UWB ranging with parameterized motion models.

(2) Bouncing Constraint

When the ball bounces before reaching the batsman (detectable from an accelerometer spike), the Z component of location – the ball’s height – is 0. This resolves the uncertainty at a single point, i.e., in combination with UWB ranging, the ball’s location can be computed *only* at this point. Thus, one point on the trajectory is “pinned down”, shortlisting a smaller set of candidate trajectories. We can now fuse these physical constraints with the underdetermined system from Fig.10.

On the other hand, there might be cases where the ball does not bounce, resulting in slight degradation in accuracy. However, sensors are being embedded in bats as well; thus, the bat’s location combined with the ball-bat contact time could serve as a virtual bounce, reducing uncertainties at a single point. This paper has not pursued such opportunities and leaves them to future work.

4.3 Fusing Range and Motion Constraints

Our goal is to model the trajectory as an error minimization problem. We denote the two anchor positions as $(x_{ia}, y_{ia}, z_{ia}) \forall i \in \{1, 2\}$. Also, we denote the initial location and initial velocity of the ball – at the point of release from the hand – as (x_o, y_o, z_o) and (v_x, v_y, v_z) , respectively. Thus, at a given time t , the estimated location of the ball from simple physics models (without aerodynamics) is:

$$S_{xe}(t) = x_o + v_x t \quad (4)$$

$$S_{ye}(t) = y_o + v_y t \quad (5)$$

$$S_{ze}(t) = z_o + v_z t - 0.5gt^2 \quad (6)$$

Here, g is the acceleration due to gravity. Using this, the

range from each anchor i is parameterized as:

$$R_{i,p}(t) = \sqrt{(S_{xe} - x_{ia})^2 + (S_{ye}(t) - y_{ia})^2 + (S_{ze}(t) - z_{ia})^2} \quad (7)$$

Once we have the range modeled, we design the error function, Err , as a difference of the parameter-modeled range and the measured range as follows.

$$\underset{6params}{\operatorname{argmin}} \quad Err = \sum_{i=1,2} \sum_t \{R_{i,p}(t) - R_{i,m}(t)\}^2 \quad (8)$$

This objective function is minimized using a gradient descent algorithm, however, since it is highly *non-convex*, multiple local maxima exist. We bound the search space based on 2 boundary conditions: (1) The Z coordinate of the bouncing location is zero. (2) The initial ball-release location is assumed to be within a $60cm^3$ cube, as a function bowler’s height.

While this proved effective in eliminating many local maxima, Fig.12(b) shows that the median ranging error is 3cm. However, translating range to location is affected by a phenomenon called *dilution of precision* (DoP) [26].

4.4 Dilution of Precision (DoP)

Ideally, the intersection of two UWB range measurements (i.e., two spheres centered at the anchors) is a circle – the ball should be at some point on this circle. In reality, ranging error causes the intersection of spheres to become 3D “tubes”. Now, when the two spheres become nearly tangential to each other, say when the ball is near the middle of two anchors, the region of intersections becomes large. Fig.13(b) shows this effect. This is called DoP and seriously affects the location estimate of the ball (later we will see how DoP in Fig.13(c) affects the localization of the players). DoP is a fundamental problem that affects other trilateration applications like GPS.

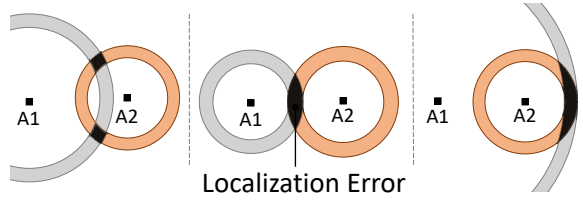


Figure 13: DoP introduced from ranging errors: (a) Lower DoP when ranging circles not tangential, (b) higher DoP when circles externally tangential, (c) max DoP when circles internally tangential.

Fig.14 shows the error variation as the ball moves in flight. The ball is released at time $t = 0$ and it reaches the batsman by the end of the flight. – clearly, the error

increases and is maximal near the middle of the flight. However, since the DoP can be modeled as a function of distance from the anchors, it should be possible to *weigh* the errors in the minimization function as follows:

$$\underset{6\text{params}}{\operatorname{argmin}} \text{ Err} = \sum_{i=1,2} \sum_t \{(R_{i,p}(t) - R_{i,m}(t)) \times \frac{1}{\sqrt{(\text{DoP})}}\}^2 \quad (9)$$

This revised minimization function pays less importance to range measurements weighted by a large DoP. Results improve to a median of 16cm error.

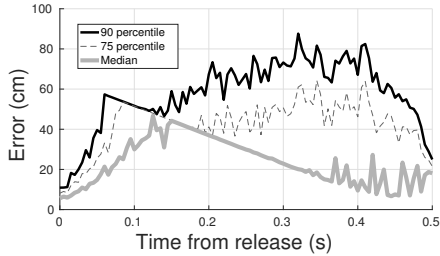


Figure 14: DoP aggravates error near the middle.

4.5 Exploiting Angle of Arrival (AoA)

The MIMO antennas at the anchors are capable of synchronized phase measurements of the incoming signal. Fig.15 shows how the phase difference ϕ is a function of the difference in signal path (p_1 and p_2), which is in turn related to AoA, θ . Thus, we have:

$$d \cos(\theta) \frac{2\pi}{\lambda} = \phi \quad (10)$$

$$\cos(AoA) = \cos(\theta) = \frac{\phi\lambda}{2\pi d} \quad (11)$$

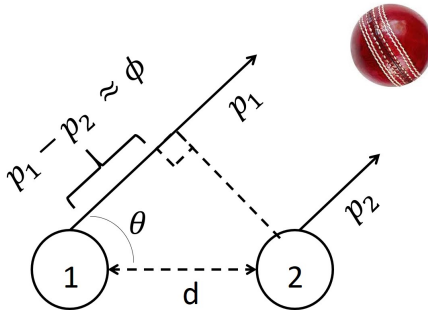


Figure 15: AoA is derived from phase differences.

We employ a MIMO receiver only on the bowler side (the other anchor cannot be utilized since it gets significantly interfered by the batsman, corrupting phase measurements). Now, for this single anchor, say the antennas are separated along the x-axis; then the AoA can be expressed in terms of ball location, anchor locations, and

measured ranges:

$$\cos(\theta) = \frac{S_x - x_{ia}}{R_{ia}} \quad (12)$$

$$S_{x,aoa} = \cos(\theta)R_{ia} + x_{ia} \quad (13)$$

Thus, it is possible to refine the previous estimates of the trajectory by including AoA in the error function. Finally, DoP problems arise with AoA too – as the ball travels further away from the anchor, the location error increases for a small $\Delta\theta$ error in AoA. In fact, the error is $R\Delta\theta$, where R is the ball’s range.

4.6 Exploiting Antenna Separation

It is clear from Equation 11 that the AoA error is a function of antenna separation d – higher antenna separation will decrease the error in measurement of $\cos \theta$ (AoA). However, with antenna separation higher than wavelength λ , the phase wraps and introduces ambiguity in AoA estimation – called *integer ambiguity*. For unambiguous AoA measurements, $d \cos \theta < \frac{\lambda}{2}$ or $d < \frac{\lambda}{2}$. Fig.16(a) shows a common case of unambiguous AoA measurement during a ball throw. Evidently, AoA is heavily corrupted from spinning antenna orientation and polarization.

To mitigate the noise, we increase the antenna separation d . However, when $d > \frac{\lambda}{2}$, the ambiguous AoA measurements are indicated in the equation below.

$$d \cos(\theta) = \frac{\phi\lambda}{2\pi} + N\lambda \quad (14)$$

$$\cos(\theta) = \frac{\phi\lambda}{2\pi d} + N \frac{\lambda}{d} \quad (15)$$

The AoA is not only a function of the phase difference ϕ , but also a function of the unknown integer ambiguity N . Fortunately, the smooth trajectory of the ball provides an opportunity for tracking the integer ambiguity across measurements, thereby any wrap around can be detected and accounted for. Fig.16(b) shows a common case of AoA measurement (known integer ambiguity) for a ball throw after increasing the antenna separation to 18 cm – 2.5 times the wavelength. Evidently, the noise is much lower, offering an additional opportunity.

4.7 Fusion of AoA with Ranging/Physics

In order to fuse, AoA, we need to firstly resolve the integer ambiguity. Our technique to resolve this is simple. At any point during the gradient search algorithm, we obtain an estimated AoA from current set of parameters. We simply resolve the integer ambiguity by substituting the currently estimated AoA in Equation 15. Incorrect ambiguity resolution would automatically explode the error function because of mismatch with range measurements.

(For example, if the integer ambiguity resolution is incorrect even by a single integer, that would introduce a median mismatch of 7.5cm (one wavelength) between inferred and measured ranges). With integer ambiguity resolution, we are ready to update the objective function Err , with AoA fusion.

$$\begin{aligned} \underset{6\text{params}}{\operatorname{argmin}} \ Err = & \sum_{i=1,2} \sum_t \left\{ (R_{i,p}(t) - R_{i,m}(t)) \times \frac{1}{\sqrt{(DoP)}} \right\}^2 \\ & + \sum_t \left\{ \frac{(S_{x,p}(t) - S_{x,aoa}(t))}{R_{aoa,p}\Delta\theta} \right\}^2 \quad (16) \end{aligned}$$

where $S_{x,aoa}(t)$ is drawn from Equation 12. The $R_{aoa,p}\Delta\theta$ (R_{aoa} denotes range from AoA anchor, $\Delta\theta$ is AoA noise) factor decreases the weight for AoA measurements taken far away from the AoA Anchor.

To summarize, iBall incorporates noisy ranging and AoA measurements from UWB Anchors with physics based motion model to track the ball trajectory. Results are presented in Section 6.

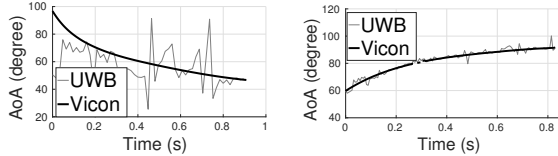


Figure 16: Improved AoA with antenna separation.

5 System Design: Player Tracking

iBall aims to track the movement of players in the field. Assuming clip-on UWB devices on the players, the ball ranging techniques should apply directly; in fact, since players are on the 2D ground, the tracking should be feasible with 2-anchor ranging alone. However, a different form of DoP emerges: when the two lines joining the player and the two anchors tend to get collinear, the ranging rings around the anchors begin to exhibit larger overlapping areas (see Fig.13(c)). Fig.17 shows simulations of DoP on a real-sized Cricket ground. As the player moves closer to the X axis (i.e., higher collinearity), the 90 percentile uncertainty of estimated location increases to 15m, in contrast to 1m when the player is perpendicular to the anchors. The effect is worse with higher distance from anchors.

5.1 DoP Suppression through Filtering

To cope with DoP degradations, we apply Kalman Filtering (KF) to player tracking. The basic idea is to detect (from the accelerometer) that a player has started running, and combine the motion model of a human-run with the UWB ranging estimates. For the human-run model, we assume the velocity to be piecewise constant

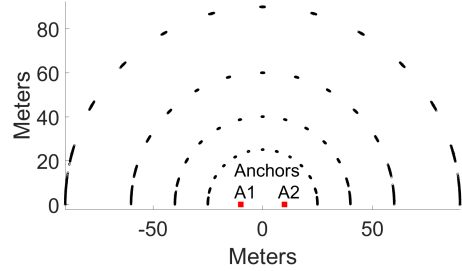


Figure 17: Simulation of estimated player location.

in short time scales (second). The velocity is periodically updated using the recent KF estimates, thereby accounting for changes in the human’s run patterns. Section 6 will show results from real experiments on a large field. iBall applies the same techniques to the ball, which can also be tracked after it has been hit by the batsman. We evaluate the overall system next.

6 Evaluation

Our experiments were performed in a $10 \times 10 \times 4 m^3$ indoor space with 8 ViCon IR cameras installed on the ceiling for ground truth (Fig.18(a)). Fig.18(b) shows IR markers pasted on the ball – this enables location and orientation tracking accuracies of $0.1mm$ and 0.2° , respectively. The authors pretended to be Cricket players and threw the ball at various speeds and spins (for a total of 100 throws). A batsman was realistically positioned to create signal blockage between the ball and the anchor. The Intel curie chip provides IMU data at $70Hz$, while the anchors perform ranging/AoA at $150Hz$.

Metrics: At any given time t during the flight of the ball, ViCon camera provides the true orientation of the ball, say $C(t)$, while iBall generates an estimated orientation, say $E(t)$. The **Orientation Error (ORE)** is essentially the minimum rotation that must be applied to $E(t)$ to align with $C(t)$. We measure this error across different values of t and plot the CDF. We also plot the angle difference between the rotation axis and the seam plane, called **Rotation Axis Error (AXE)** and **Seam Plane Error (PLE)**. Now, the true angular velocity of the ball, C_ω can be computed as $\frac{C(t_2)C(t_1)^{-1}}{t_2-t_1}$ (note that difference in orientation matrices is computed through inverse functions). When multiplied by the time of the flight, the result is the total cumulative angle truly rotated by the ball. We compute the same from $E(t)$ and ultimately compute the difference in the **Cumulative Angle Error (CUE)**. To understand the impact of higher spin, we also report the orientation error (OE) for varying angular velocity. For trajectory, the metrics are simpler, namely **Location Error (LOE)** and **Speed Error (SPE)** reported against various parameters.



Figure 18: (a) IR based ViCon cameras at the ceiling. (b) A cricket ball instrumented with IR markers.

6.1 Performance of Spin Tracking

(1) Cumulative Angle Error (CUE): Fig.19 reports the CUE for each of the 50 spin throws – the results are sorted in ascending order of cumulative angles. A Y axis value of 4000 implies that the ball has rotated $\frac{4000}{360}$, which is 11.1 cycles in air at the end of the flight. Evidently, iBall performs close to the Vicon ground truth for almost every throw. More importantly, unlike gyroscopes (which suffer from drift), the magnetometer does not accumulate error over time (since it measures the absolute North vector at every sample). This is a promising result and a valuable primitive for various types of ball analytics.

Error in estimated angular velocity (not shown) follows the same trend as Fig.19(a), since it is simply the cumulative rotation divided by flight time. Across 50 experiments, we observe median angular velocity error of 1.0% and a maximum error of 3.9%.

(2) Overall Orientation Error (ORE): Fig.19(b) reports the CDF of ORE across all 50 throws – the median is 11.2° . We also break down this error into local rotation axis error (AXE) and seam plane orientation error (PLE). We are especially interested in these two because accurately controlling rotation axis and seam plane is critical in maintaining the stability of the ball in the air. Results show a median AXE of $< 5^\circ$ and a median PLE of $< 8^\circ$, while the 90th percentile remains $< 20^\circ$.

(3) Impact of High Spin: Fig.19(c) reports the impact of higher spin on ORE. The accuracy slightly degrades as the angular velocity increases. This is because, at higher angular velocity, our estimation of global rotation axis \hat{R}^G is less accurate, degrading ORE. However, since the flight time is short, the accuracy degradation is marginal.

6.2 Performance of Trajectory Tracking

(1) Overall Location Error (LOE): Fig.20(a) quantifies the location error (LOE) across 50 different throws – the median error is 8cm. We also report the errors on each of the directions: Y in the direction of the throw, Z being

vertically upwards, and X is perpendicular to Y and Z. The median X, Y, and Z axes errors are 4.5cm, 3.4cm and 2.39cm respectively. The X axis errors are maximum due to DoP effects, however, AoA lowers it to a reasonable value.

3 Does LOE Accumulate at the End of the Flight?

Fig.20(b) shows the median, 25th, and 75th percentile error for different positions of the ball during the flight. Importantly, since we solve a global error minimization problem, the error does not accumulate. Still, the initial positions have higher accuracy compared to the end of the flight because AoA computed from the bowler-side anchor exhibits significantly less error. The degradation is still modest, with a median end-flight LOE of 15cm.

(3) Speed Error (SPE) and Impact of Speed: iBall computes velocity estimates – Fig.20(c) shows a median speed error (SPE) of 0.4m/s. Upon discussions with domain experts, we gather that this level of accuracy is valuable for coaching and analytics. Fig.21(a) decomposes the overall LOE results into different speed buckets. Evidently, the accuracy does not degrade at higher speed regimes (the maximum speed we could achieve in our experiments was 22m/s). Of course, this is indoors and wind effects are minimal, if any.

(4) Trajectory Extrapolation: The ball sometimes hits the leg of the batsman. An important question in Cricket is: *would the ball hit the wicket if the batsman was not in the way?* This is called *leg before wickets (LBW)*. For LBW decisions, it's valuable to be able to predict (or extrapolate) the trajectory of the ball. The International Cricket Association has declared 10cm as the minimum tolerable LOE for LBW decisions. Fig.21(b) shows the trajectory prediction error with iBall. While the 3D LOE is 22cm, the x-axis error is smaller (9.9cm), indicating the feasibility of using iBall for LBW decisions.

6.3 Performance of Player Tracking

Fig.21(c) shows LOE when the player is running at different parts of the playground – each line in the graph corresponds to the angle made by the lines joining the player and the two anchors. This also represents the LOE of the ball after it has been hit. We experimented in a real playground with a user running in a precise peripheral circle of 89m radius. At low angles (i.e., running almost collinear with the two anchors), the 90th percentile error can be as large as 3.5m. Our Kalman Filter based approach reduces this LOE to 2.6m, while at higher angles, the LOE is already less than 50cm.

7 Discussion and Future Work

(1) Scaling to greater speed and spin: Our maximum throw speeds were limited by our own abilities. Perhaps

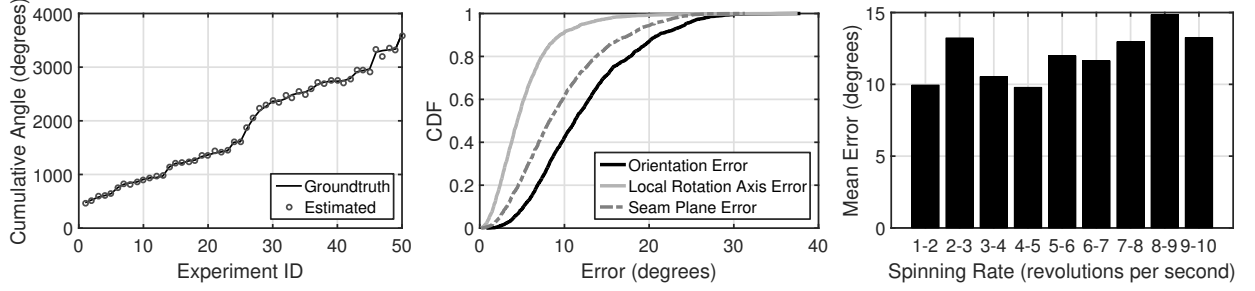


Figure 19: (a) Cumulative angle error (CUE) across different experiments. (b) CDF of orientation error (ORE). (c) Average orientation tracking error (ORE) under different spinning rate.

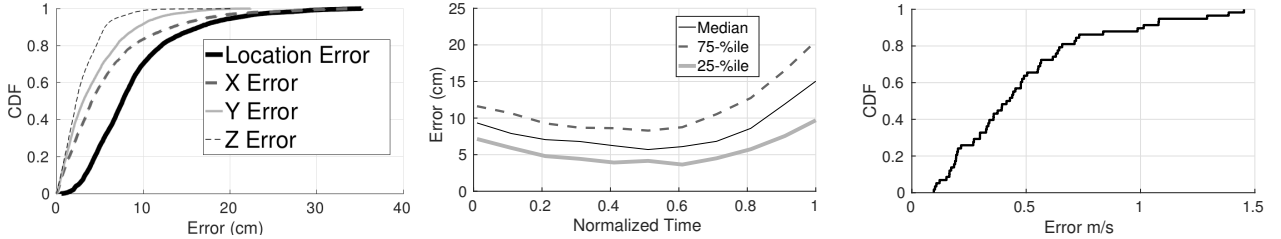


Figure 20: (a) CDF of location tracking errors. (b) iBall’s location error degrades slightly toward the end of ball flight. (c) CDF of ball speed error.

a bowling machine would serve as a better experimentation platform. For spin, limitations arose from ViCon – we observed increasing jitters and discontinuities in the ViCon data for spins above 12rps . We are exploring alternative ground-truth estimation techniques at such spin regimes.

(2) Indoor experiments: We need experimentation under outdoor aerodynamic effects – the reported results may have been favorable in its absence. The lack of an outdoor ground truth system has been the bottleneck so far – we are exploring alternatives.

(3) Multipath: On the other hand, indoor environments may have affected the AoA estimates as well. In an outdoor setting, wireless multipath is expected to be less pronounced, potentially offering better reliability with AoA estimation and fusion.

(4) Generalizing to other sports: We believe iBall’s techniques can be extended to other sports with domain specific modifications. For example, stitches on a baseball induce different aerodynamic effects, however, these differences can be modeled and incorporated into iBall. Such models are also available for golf and tennis balls, allowing them to be suitably “plugged” into our framework. Finally, iBall’s techniques may extend to hollow balls like soccer and basketball. Adidas micoach [2] has designed a soccer ball with multiple suspended sensors within the ball. This can potentially offer more information to iBall’s optimization engine.

(5) Smart ball weight distribution: Needless to say, our ball prototype is not ready for real use – the embedded sensor is not optimized to preserve the homogeneous mass distribution inside the ball. This may have led to some biases in the trajectory and spin results, although we believe it is marginal. In the longer run, mechanical engineering experts from D2M [3] have corroborated that a near ideal weight distribution (with impact tolerance) is feasible. The opportunities arise from smaller spatial footprint of the device, eliminating the battery (by harvesting energy from the ball’s spin), and combining the IMU and the radio in a single smaller chip. Validating our results on such a professionally manufactured ball remains a part of future work.

(6) Enhancing accuracy: We believe there is room to improve the location and spin tracking accuracy of iBall. For example, it should be possible to jointly estimate the location and rotation instead of treating them as separate modules. The accelerometer can measure a combination of centripetal force (rotation) and linear acceleration. Similarly, the UWB ranging measurements contain a few bits of information about the orientation since the radios cannot be precisely placed at the center of mass of the ball. Such a coupling suggests that joint estimation of can improve the accuracy of both. Hardware opportunities that leverage dual carrier UWB receivers can further decrease errors in AoA, perhaps at a slight increase in hardware complexity.

(6) Battery life and connectivity: The current ball pro-

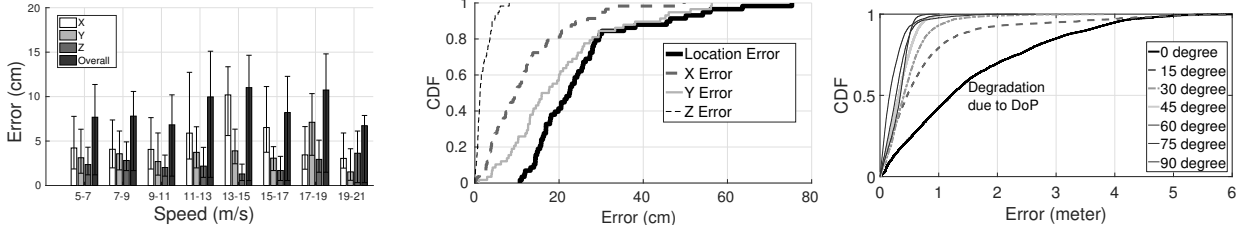


Figure 21: (a) LOE across ball speeds. (b) Prediction accuracy sufficient for LBW. (c) Player location error.

totype allows a battery life of $\approx 75 - 90$ minutes between recharges, permitting short training sessions. In future, perhaps wireless charging will mitigate this problem; perhaps fast rotation will automatically scavenge energy. Additional energy optimizations could be made in the compute as well as the communication pipeline, i.e., when the ball sends the sensor data to the anchor. As one simple example, the anchors could perhaps beam-form towards the ball to minimize the ball’s transmission energy. Since the anchor is equipped with a large battery, such asymmetric designs should be viable.

8 Related Work

Embedded IMU: Authors in [19, 17, 18, 32] embed IMUs in a Cricket ball and is perhaps closest to our work. However, these (brief) papers report basic features such as angular velocity, time of flight, etc. These features are directly available from the sensors and do not address the actual metrics of interest to the players/coaches. Authors in [16] also embed IMUs but focus mainly on the design and packaging of the ball for high impact. [24] explores spin-analytics in the context of a Bowling ball, however, due to low spin-rates and contact with the floor, accelerometers and gyroscopes are readily usable. This simplifies the problem in contrast to Baseball and Cricket.

Wearables, Cameras, and Sports Analytics: Several startups like Zepp, MiCoach, and Ball are extracting motion patterns from wearables. Smart sensor shoes have been proposed for analyzing soccer shots in [47], however, these are essentially classification problems. Hawk-Eye [7] is perhaps the most popular and expensive camera based tracker officially adopted in Cricket, Tennis, etc. Hot Spot [10] is a popular IR technology used to determine contact points between ball and players. Video analytics efforts in [23, 37, 46] are processing video feeds to learn/predict game strategies. While creative, the projects are addressing a different set of problems.

Localization and Motion Tracking: Rich literature in indoor localization [13, 45, 15, 43, 33, 42, 36, 41, 25] has mostly focused on human motion. Under sparse WiFi infrastructure and high ball speeds, such techniques are inadequate. UWB based ToF ranging [31] report 10cm

accuracy for static objects. We build on this technique but fuse with AoA, motion models, and DoP constraints, to cope with real-world challenges. On a similar note, inertial sensor based tracking have mostly been performed on humans, robots and drones [29, 30, 48, 28, 27, 35]. However, unlike iBall, none of these works address the space of freely falling objects. While work in [38] tracks ballistic missiles, the granularity of tracking is different both in time and space. iBall entails much finer granularities of tracking and appropriately formulates a global optimization problem for better accuracy unlike filtering techniques in [38].

9 Conclusion

This paper develops techniques for tracking the 3D trajectory and spin parameters of a cricket ball. The core problem is rooted in motion tracking techniques, however, the sporting applications (and Cricket in this case) presents unique challenges and opportunities. Through fusion of wireless ranging, models of free-falling objects, and angle of arrival estimates, we formulate and solve error minimization problems. Results are promising and we expect our techniques to generalize to other sports. Our ongoing work is in pursuit of baseball and frisbee.

10 Acknowledgments

We sincerely thank our shepherd Dr. Anirudh Badam and the anonymous reviewers for their valuable feedback. We are also grateful to NSF (CNS - 1423455) for partially funding the research. We acknowledge the support of various teams in bringing the system together. 1) Hardware and Software engineers at Intel[11] for helping on various design aspects of the embedded sensor hardware and software. 2) D2M[3] for ball design and prototyping. 3) The International Cricket Council (ICC) [12] and Narayan Sundararajan for providing domain expertise on the game of cricket and the business of sports analytics. 4) The Intelligent Robotics Lab (IRL) at UIUC for providing access to ViCon lab space.

References

- [1] <http://www.jamesgibbard.co.uk/electronics/bluetoothcontrolledledflashingfrisbee>.

- [2] adidas micoach smart ball. <http://www.adidas.com/us/micoach-smart-ball/G83963.html>.
- [3] D2m. <http://d2m-inc.com/>.
- [4] Decawave.
- [5] Firstv1sion. <http://www.firstvision.com/en/product/>.
- [6] Goal-line technology. https://en.wikipedia.org/wiki/Goal-line_technology.
- [7] Hawk-eye. [https://en.wikipedia.org/wiki/Hawk-Eye/](https://en.wikipedia.org/wiki/Hawk-Eye).
- [8] High range gyroscopes. <http://www.analog.com/en/products/mems/gyroscopes.html>.
- [9] High speed camera. <http://www.untamedscience.com/filmmaking/advanced-filmmaking/high-speed-video-slow-motion/>.
- [10] Hot spot. [https://en.wikipedia.org/wiki/Hot_Spot_\(cricket\)](https://en.wikipedia.org/wiki/Hot_Spot_(cricket)).
- [11] Intel, data center solutions, iot and pc innovation. <http://www.intel.com>.
- [12] International cricket council. <http://www.icc-cricket.com>.
- [13] BAHL, P., AND PADMANABHAN, V. N. Radar: An in-building rf-based user location and tracking system. In *INFOCOM 2000. Nineteenth Annual Joint Conference of the IEEE Computer and Communications Societies. Proceedings. IEEE* (2000), vol. 2, Ieee, pp. 775–784.
- [14] BAKER, C. A calculation of cricket ball trajectories. *Proceedings of the Institution of Mechanical Engineers, Part C: Journal of Mechanical Engineering Science* 224, 9 (2010), 1947–1958.
- [15] CHINTALAPUDI, K., PADMANABHA IYER, A., AND PADMANABHAN, V. N. Indoor localization without the pain. In *Proceedings of the sixteenth annual international conference on Mobile computing and networking* (2010), ACM, pp. 173–184.
- [16] FUSS, F., FERDINANDS, R., DOLJIN, B., AND BEACH, A. Development of a smart cricket ball and advanced performance analysis of spin bowling. In *ICSST 2014: Advanced Technologies in Modern Day Sports* (2014), Institute for Sports Research (ISR), pp. 588–595.
- [17] FUSS, F. K., LYTHGO, N., SMITH, R. M., BENSON, A. C., AND GORDON, B. Identification of key performance parameters during off-spin bowling with a smart cricket ball. *Sports Technology* 4, 3-4 (2011), 159–163.
- [18] FUSS, F. K., AND SMITH, R. M. Accuracy performance parameters of seam bowling, measured with a smart cricket ball. *Procedia Engineering* 72 (2014), 435–440.
- [19] FUSS, F. K., SMITH, R. M., AND SUBIC, A. Determination of spin rate and axes with an instrumented cricket ball. *Procedia Engineering* 34 (2012), 128–133.
- [20] GUPTA, S., MORRIS, D., PATEL, S., AND TAN, D. Soundwave: using the doppler effect to sense gestures. In *Proceedings of the SIGCHI Conference on Human Factors in Computing Systems* (2012), ACM, pp. 1911–1914.
- [21] HACH, R. Symmetric double sided two-way ranging. *IEEE P802 15* (2005), 802–15.
- [22] HAHNEL, D., BURGARD, W., FOX, D., AND THRUN, S. An efficient fastslam algorithm for generating maps of large-scale cyclic environments from raw laser range measurements. In *Intelligent Robots and Systems, 2003.(IROS 2003). Proceedings. 2003 IEEE/RSJ International Conference on* (2003), vol. 1, IEEE, pp. 206–211.
- [23] HALVORSEN, P., SÆGROV, S., MORTENSEN, A., KRISTENSEN, D. K., EICHHORN, A., STENHAUG, M., DAHL, S., STENSLAND, H. K., GADDAM, V. R., GRIWODZ, C., ET AL. Bagadus: an integrated system for arena sports analytics: a soccer case study. In *Proceedings of the 4th ACM Multimedia Systems Conference* (2013), ACM, pp. 48–59.
- [24] KING, K., PERKINS, N. C., CHURCHILL, H., MCGINNIS, R., DOSS, R., AND HICKLAND, R. Bowling ball dynamics revealed by miniature wireless mems inertial measurement unit. *Sports Engineering* 13, 2 (2011), 95–104.
- [25] KUMAR, S., GIL, S., KATABI, D., AND RUS, D. Accurate indoor localization with zero start-up cost. In *Proceedings of the 20th annual international conference on Mobile computing and networking* (2014), ACM, pp. 483–494.
- [26] LANGLEY, R. B. Dilution of precision. *GPS world* 10, 5 (1999), 52–59.
- [27] LEFFERTS, E. J., MARKLEY, F. L., AND SHUSTER, M. D. Kalman filtering for spacecraft attitude estimation. *Journal of Guidance, Control, and Dynamics* 5, 5 (1982), 417–429.
- [28] LIANG, W. Y., MIAO, W. T., HONG, L. J., LEI, X. C., AND CHEN, Z. Attitude estimation for small helicopter using extended kalman filter. In *Robotics, Automation and Mechatronics, 2008 IEEE Conference on* (2008), IEEE, pp. 577–581.
- [29] MADGWICK, S. An efficient orientation filter for inertial and inertial/magnetic sensor arrays. *Report x-io and University of Bristol (UK)* (2010).
- [30] MAHONY, R., HAMEL, T., AND PFLIMLIN, J.-M. Nonlinear complementary filters on the special orthogonal group. *IEEE Transactions on Automatic Control* 53, 5 (2008), 1203–1218.
- [31] MCELROY, C., NEIRYNCK, D., AND McLAUGHLIN, M. Comparison of wireless clock synchronization algorithms for indoor location systems. In *2014 IEEE International Conference on Communications Workshops (ICC)* (2014), IEEE, pp. 157–162.
- [32] MCGINNIS, R. S., AND PERKINS, N. C. A highly miniaturized, wireless inertial measurement unit for characterizing the dynamics of pitched baseballs and softballs. *Sensors* 12, 9 (2012), 11933–11945.
- [33] NICULESCU, D., AND NATH, B. Ad hoc positioning system (aps) using aoa. In *INFOCOM 2003. Twenty-Second Annual Joint Conference of the IEEE Computer and Communications. IEEE Societies* (2003), vol. 3, Ieee, pp. 1734–1743.
- [34] NIKE. Footwear having sensor system. Patent US 8676541 B2.
- [35] PFLIMLIN, J. M., HAMEL, T., AND SOUÈRES, P. Nonlinear attitude and gyroscope's bias estimation for a vtol uav. *International Journal of Systems Science* 38, 3 (2007), 197–210.
- [36] RAI, A., CHINTALAPUDI, K. K., PADMANABHAN, V. N., AND SEN, R. Zee: zero-effort crowdsourcing for indoor localization. In *Proceedings of the 18th annual international conference on Mobile computing and networking* (2012), ACM, pp. 293–304.
- [37] SEO, Y., CHOI, S., KIM, H., AND HONG, K.-S. Where are the ball and players? soccer game analysis with color-based tracking and image mosaic. In *International Conference on Image Analysis and Processing* (1997), Springer, pp. 196–203.
- [38] SIOURIS, G. M., CHEN, G., AND WANG, J. Tracking an incoming ballistic missile using an extended interval kalman filter. *IEEE Transactions on Aerospace and Electronic Systems* 33, 1 (1997), 232–240.
- [39] SWANSON, E. Geometric dilution of precision. *Navigation* 25, 4 (1978), 425–429.
- [40] TSAI, N.-C., AND SUE, C.-Y. Stability and resonance of micro-machined gyroscope under nonlinearity effects. *Nonlinear Dynamics* 56, 4 (2009), 369–379.

- [41] VASISHT, D., KUMAR, S., AND KATABI, D. Decimeter-level localization with a single wifi access point. In *13th USENIX Symposium on Networked Systems Design and Implementation (NSDI 16)* (2016), pp. 165–178.
- [42] WANG, H., SEN, S., ELGOHARY, A., FARID, M., YOUSSEF, M., AND CHOUDHURY, R. R. No need to war-drive: unsupervised indoor localization. In *Proceedings of the 10th international conference on Mobile systems, applications, and services* (2012), ACM, pp. 197–210.
- [43] XIONG, J., AND JAMIESON, K. Arraytrack: a fine-grained indoor location system. In *Presented as part of the 10th USENIX Symposium on Networked Systems Design and Implementation (NSDI 13)* (2013), pp. 71–84.
- [44] YANG, L., CHEN, Y., LI, X.-Y., XIAO, C., LI, M., AND LIU, Y. Tagoram: Real-time tracking of mobile rfid tags to high precision using cots devices. In *Proceedings of the 20th annual international conference on Mobile computing and networking* (2014), ACM, pp. 237–248.
- [45] YOUSSEF, M., AND AGRAWALA, A. The horus wlan location determination system. In *Proceedings of the 3rd international conference on Mobile systems, applications, and services* (2005), ACM, pp. 205–218.
- [46] YU, X., XU, C., LEONG, H. W., TIAN, Q., TANG, Q., AND WAN, K. W. Trajectory-based ball detection and tracking with applications to semantic analysis of broadcast soccer video. In *Proceedings of the eleventh ACM international conference on Multimedia* (2003), ACM, pp. 11–20.
- [47] ZHOU, B., KOERGER, H., WIRTH, M., ZWICK, C., MARTIN-DALE, C., CRUZ, H., ESKOFIER, B., AND LUKOWICZ, P. Smart soccer shoe: monitoring foot-ball interaction with shoe integrated textile pressure sensor matrix. In *Proceedings of the 2016 ACM International Symposium on Wearable Computers* (2016), ACM, pp. 64–71.
- [48] ZHOU, P., LI, M., AND SHEN, G. Use it free: instantly knowing your phone attitude. In *Proceedings of the 20th annual international conference on Mobile computing and networking* (2014), ACM, pp. 605–616.